

Chapter 4

Design and experimental set up of a Differential Scanning Calorimeter with magnetic field

4.1 Introduction

Calorimetry has been used to study a number of physical properties of solids for more than a century [1]. Even now, it is considered to be one of the best suited methods to determine the nature of phase transitions. Nowadays, a wide variety of calorimeters exist, which can be broadly classed into two groups. The first group includes those devices which measure the heat flow between the sample and a thermal block, while the temperature of the calorimeter is continuously changed (scanning calorimeters). Most of them use a dummy sample so that they work differentially (differential scanning calorimeters, DSC). The second group includes the calorimeters which are based on the measurement of the temperature of the sample after a small amount of heat is supplied (adiabatic calorimetry, relaxation calorimetry and ac calorimetry). In these instruments, the temperature of the calorimeter is kept constant during the measurement. There are also calorimeters which combine the two operating methods, as for instance in case of the modulated differential scanning calorimeters which have been recently developed [2]. Continuous efforts are devoted to designing calorimeters that are better adapted to the new materials and with better performances [3, 4].

DSCs are particularly suited to studying first-order phase transitions since they measure the heat flow, and a proper integration of the calibrated signal yields the latent heat of the transition. In contrast, a.c., relaxation and adiabatic calorimetry are suitable for determining the heat capacity C_p and hence are well adapted for studying continuous phase transitions. It should be noted that in a first-order

transition, a heat input does not result in a modification of the temperature of the sample and, therefore, the latter techniques are not suitable for studying this kind of phase transitions.

The determination of the entropy change associated with the magnetocaloric effect in $\text{Gd}_5(\text{Si}_x\text{Ge}_{1-x})_4$ series of alloys has been an issue of controversial debate [5, 6, 7, 8, 9], since the effect occurs in the vicinity of the first-order magnetostructural transition (see section 2.7). As discussed in section 1.3, the adiabatic temperature change can be evaluated both indirectly through $C_p(T, H)$ measurements, which are usually obtained with quasiadiabatic calorimeters [10]), and directly with specially designed devices [11, 12]. However, the entropy change can only be obtained indirectly using $C_p(T, H)$ measurements, which are not valid in the vicinity of first-order transitions, or magnetisation measurements, and even in this case the correct approach is not clear (section 2.7). Nevertheless, if the entropy change arises from a first-order transition, DSC enables us to measure it in a more direct manner. Furthermore, since MCE appears in a first-order transition only if the latter can be field-induced, DSC under applied magnetic field is thus expected to be the ideal technique to study the entropy change at first-order magnetostructural transitions. In this chapter, we describe a high-sensitivity differential scanning calorimeter specially designed to operate over a temperature range from 10 to 300 K and under magnetic fields of up to 5 T. This calorimeter provides accurate values of the latent heat and entropy change under magnetic field at a first order phase transition.

4.2 Experimental Details

The calorimeter can be adapted to any cryostat equipped with a superconducting magnet. The apparatus described here has the appropriate size to be used with a Teslatron© (Oxford Instruments) system as a host platform (see Fig. 4.1). A magnetic field of up to 5 T is generated along the vertical axis by a superconducting magnet contained in the Teslatron system. Figure 4.2 shows side (a) and top (b) cross sections of the calorimeter. The calorimeter is a copper spool (1)¹. It is mechanically clamped to a long stainless steel tube. All wiring is routed through this rod and exits the system via an electrical feedthrough at its far end. The two sensors (2), which are differentially connected, are placed on the flattened inner surfaces of the spool. In order to ensure a good thermal contact, the sensors are coupled to the block with General Electrics Oxford Varnish. These sensors are batteries of thermocouples (Melcor FCO.45-32-05L)² made of P-N- junctions of

¹For optimal performance, the mass of the spool has to be large enough so that its specific heat amounts at least 100 times that of the sample (or reference).

²©Melcor Thermoelectrics, 1040 Spruce st., Trenton, NJ; 08648.

4.2. Experimental Details

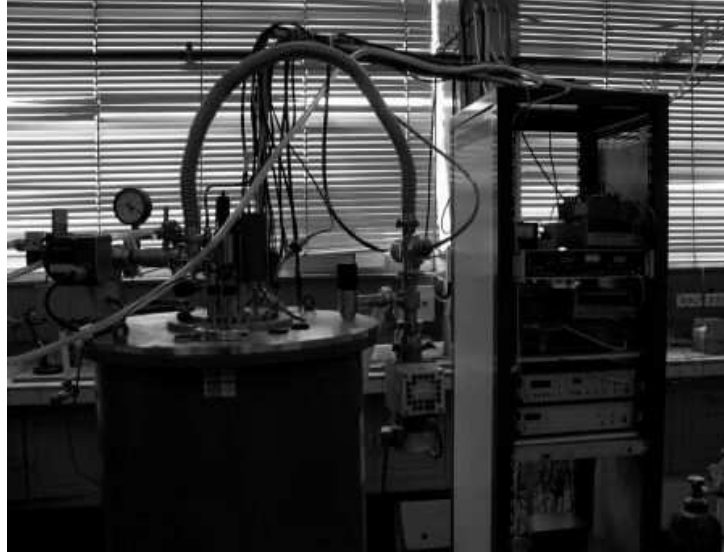


Figure 4.1: Overview of the Teslatron© (Oxford Instruments) cryomagnetic system operating with LHe from 1.5 to 300 K. The cryostat holds a superconducting coil which generates magnetic fields up to 5 T. Electronics of the device can be seen at the right-hand side.

Bi_2Te_3 (32 pairs of junctions on a $6.5 \times 6.5 \text{ mm}^2$ surface). Sample (3) and inert reference (4) are placed directly on top of each sensor. They are held in place (in good thermal contact with the sensor) by winding a thin (less than 0.2 mm diameter) nylon wire around the assembly. Electrical wires exit the calorimeter through 2.5 mm diameter holes, and they are thermally coupled to the upper part of the spool before passing through the stainless steel rod. Such a coupling avoids the existence of thermal gradients on the wires which could give rise to spurious thermoelectric voltages. The temperature of the calorimeter is scanned by changing the temperature of the variable temperature insert (VTI) of the Teslatron cryostat [13]. An accurate reading of the actual temperature of the calorimeter is achieved by monitoring the electrical resistance of a Carbon-glass resistor (LakeShore Cryotronics INC. CGR-1-500) (5) embedded inside the spool. In order to minimise convection of the exchange gas inside the calorimeter, the whole assembly is covered by an external copper cylinder (1 mm thick) (6), which is screwed to the upper part of the spool. For an optimal operation, the pressure inside the calorimeter should be within the range 200-600 mbar [13]. High purity helium is required since impurities affect the sensitivity of the calorimeter.

The heat released (or absorbed) by the sample (see Fig. 4.2(c)) is measured by reading the voltage furnished by the thermobatteries (electrical output) by using a nanovoltmeter (Keithley 182). It is worth reminding that, since the two sensors

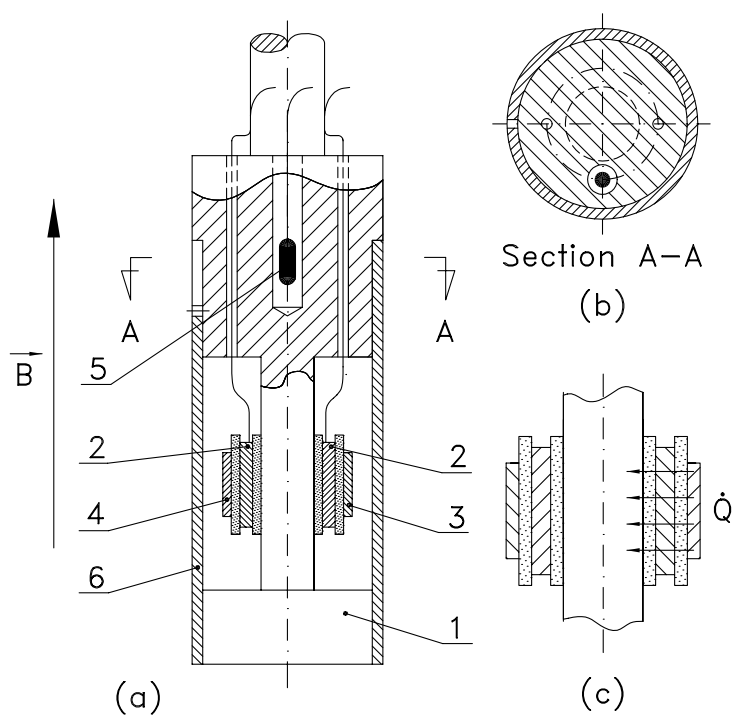


Figure 4.2: Side (a) and top (b) view cross sections of the calorimeter. (1) Copper spool, (2) sensors, (3) sample, (4) reference, (5) carbon-glass resistor and (6) cover. The magnetic field, $\vec{B} = \mu_0 \vec{H}$, is applied along the symmetry axis of the calorimeter. (c) Detail showing the heat flow \dot{Q} for an exothermal transition.

4.3. Calibration



Figure 4.3: View of the probe with the differential scanning calorimeter (copper spool) at the right-hand side, adapted to be used with the Teslatron cryomagnetic system.

are connected differentially, the drift in the calorimetric output associated with changes in the temperature of the calorimetric block are minimised by the fact that the heat flow of the reference is subtracted from that of the sample, and therefore, the major contribution to the calorimetric output is the thermal power released (or absorbed) by the sample during the first order phase transition (latent heat). The resistance of the carbon-glass is read by means of a lock-in amplifier (EG & G 7260)³. The whole system (including the electronics of the Teslatron measurement system) is controlled by a PC computer. Values of voltage $V(t)$ and temperature $T(t)$ are acquired at typical rates of 0.25 Hz. A view of the calorimeter is shown in Figs. 4.3 and 4.4.

4.3 Calibration

Since the thermocouples are made of semiconducting elements, the magnetic field is not expected to affect their thermoelectric output. In contrast, the output voltage will indeed significantly depend on temperature and therefore, a proper calibration over the whole operating temperature range is needed. To carry out such a calibration, the sample is replaced by a manganin resistance (50Ω). A constant power (W) is dissipated by the Joule effect at the resistance (without the applied magnetic field), and the electrical output at the steady state, Y , is measured. The sensitivity, K , is then given by: $K = Y/W$. A typical calorimetric curve for $W=18$ mW is shown in the inset of Fig. 4.5⁴. The values obtained for the sensitivity at different temperatures are plotted in Fig. 4.5. Data can be fitted by the curve: $K(\text{mV/W})=1.4 \times 10^{-8}T^4 - 2.0 \times 10^{-5}T^3 + 5.1 \times 10^{-3}T^2 + 0.86T$, which is also

³A microvoltmeter can also be used to read the resistance of the thermometer.

⁴The linearity of the calorimeter has been verified by performing calibrations with different values of the released power.



Figure 4.4: Detail of the differential scanning calorimeter.

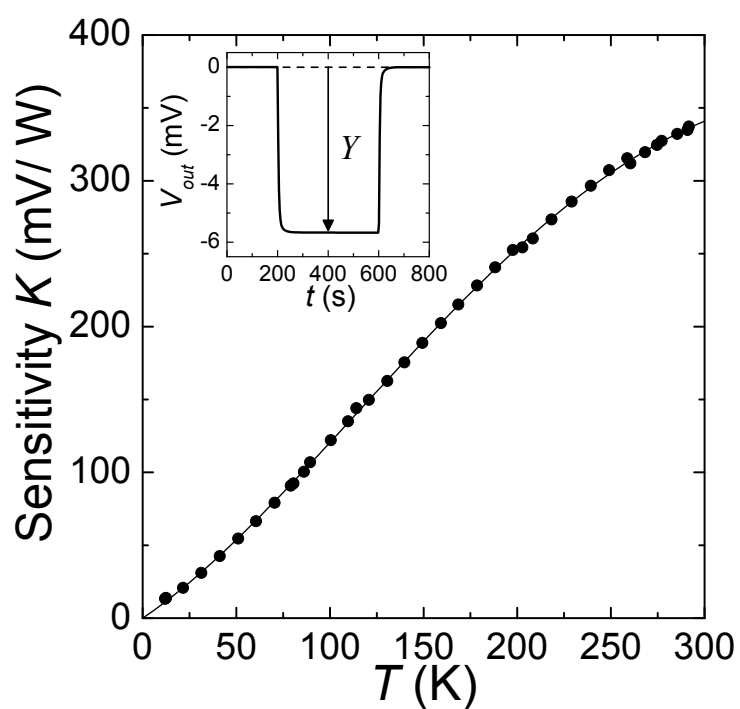


Figure 4.5: Sensitivity at zero field as a function of temperature. The solid line is a fit to the data. Inset: example of a typical calibration thermogram at $T=173$ K.

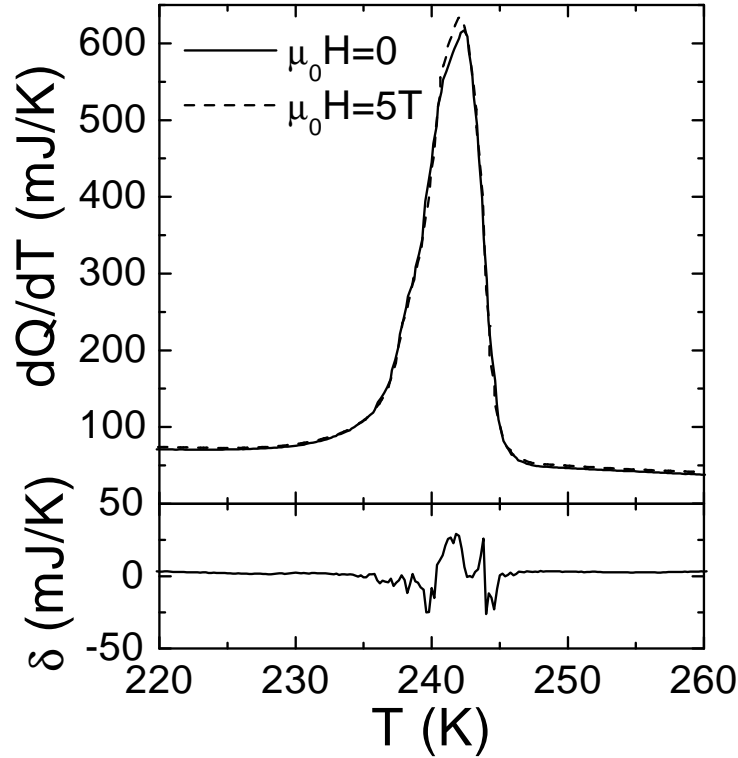


Figure 4.6: Calorimetric curves recorded at the martensitic transition of a $\text{Cu}_{2.717}\text{Zn}_{0.646}\text{Al}_{0.637}$ single crystal at zero field (continuous curve) and at $\mu_0 H = 5$ T (discontinuous curve). The difference between these two curves δ is also shown.

plotted in the figure. It is interesting to note that the room temperature value is around 10 times larger than the sensitivity for a conventional DSC [14], and that at temperatures as low as 10 K, a reasonably high value is still obtained.

To check the performances of the calorimeter, we have selected a Cu-Zn-Al alloy undergoing a structural (martensitic) transition, as a standard system. This material is diamagnetic and hence the transition is not affected by a magnetic field; this will provide a good test of the insensitivity of the sensors to a magnetic field. On the other hand, the values for the latent heat and entropy change associated with the martensitic transition are very well established over a broad temperature range by the use of several experimental techniques (the transition temperature can be modified by slightly tuning the composition) [15, 16]. The calorimetric curves recorded during the reverse transition of a Cu-Zn-Al crystal are shown in Fig. 4.6, in the absence of a magnetic field (continuous line) and for an applied field of 5 T (discontinuous curve). Since the two curves are almost indistinguishable, we have also plotted the difference between them, δ . No significant influence of the magnetic field is observed.

In order to obtain the latent heat and the entropy change in a first-order phase transition, we calculate the heat flow as $\dot{Q}(t)=V(t)/K$, we compute numerically the heating/cooling rate dT/dt from the recorded $T(t)$ and finally the calorimetric curve $dQ/dT=\dot{Q} (dT/dt)^{-1}$ is achieved. This calorimetric signal has to be corrected from the baseline (details can be found, for instance, in Ref. [17]). The latent heat and the entropy change are then given by:

$$L = \int_{T_L}^{T_H} \frac{dQ}{dT} dT ; \quad \Delta S = \int_{T_L}^{T_H} \frac{1}{T} \frac{dQ}{dT} dT , \quad (4.1)$$

where T_H and T_L are respectively temperatures above and below the starting and finishing transition temperatures. The values obtained for the latent heat [$L(\mu_0H=0)=336 \pm 3$ J/mol and $L(\mu_0H=5T)=335 \pm 3$ J/mol] and for the entropy change [$\Delta S(\mu_0H=0)=1.40 \pm 0.01$ J/(mol K) and $\Delta S(\mu_0H=5T)=1.39 \pm 0.01$ J/(mol K)] at the martensitic transition of Cu-Zn-Al are in excellent agreement with published values [15, 16].

4.4 Results sweeping T

The apparatus described in the present chapter is particularly well adapted for measuring the entropy change at the magnetostructural phase transition undergone by alloys which exhibit the giant magnetocaloric effect. Proper measurement of the entropy change associated with the first-order transition is expected to contribute to a better understanding of this interesting phenomenon, in particular for $Gd_5(Si_xGe_{1-x})_4$ series of alloys. Figure 4.7 shows an example of the thermal curves recorded during heating and cooling (i.e., sweeping T) of a $Gd_5(Si_{0.1}Ge_{0.9})_4$ sample under different applied magnetic fields. The small λ -peak at around 130 K arises from the second-order $PM \leftrightarrow AFM$ phase transition. The large peak at lower temperatures is due to the first-order phase transition between two different orthorhombic structures [$O(II) \leftrightarrow O(I)$], that occurs simultaneously with a magnetic $AFM \leftrightarrow FM$ transition (see Refs. [18, 19] and section 2.2). The thermal hysteresis amounts to 2-3 K. The magnetic field dependence of the first-order phase transition is evident from the calorimetric curves. The transition temperature, T_t , linearly increases with the magnetic field, with a slope $(dT_t/d(\mu_0H_t))=4.1 \pm 0.1$ K/T) which is in agreement with that derived from magnetisation measurements [19]. The entropy change at the transition has also been found to increase with magnetic field, as shown in the insets of Fig. 4.7. For $\mu_0H=0$, $\Delta S=-24.2$ J/(kg K) [-2.85 J/(mol K)] while for $\mu_0H=5$ T, $\Delta S=-33.7$ J/(kg K) [-3.96 J/(mol K)], on cooling. Results on heating yield the same behavior, with ΔS absolute values slightly lowered with respect on cooling [by ~ 0.7 J/(kg K)]. Such a large increase of the entropy change with T is a consequence of the coupling between structural

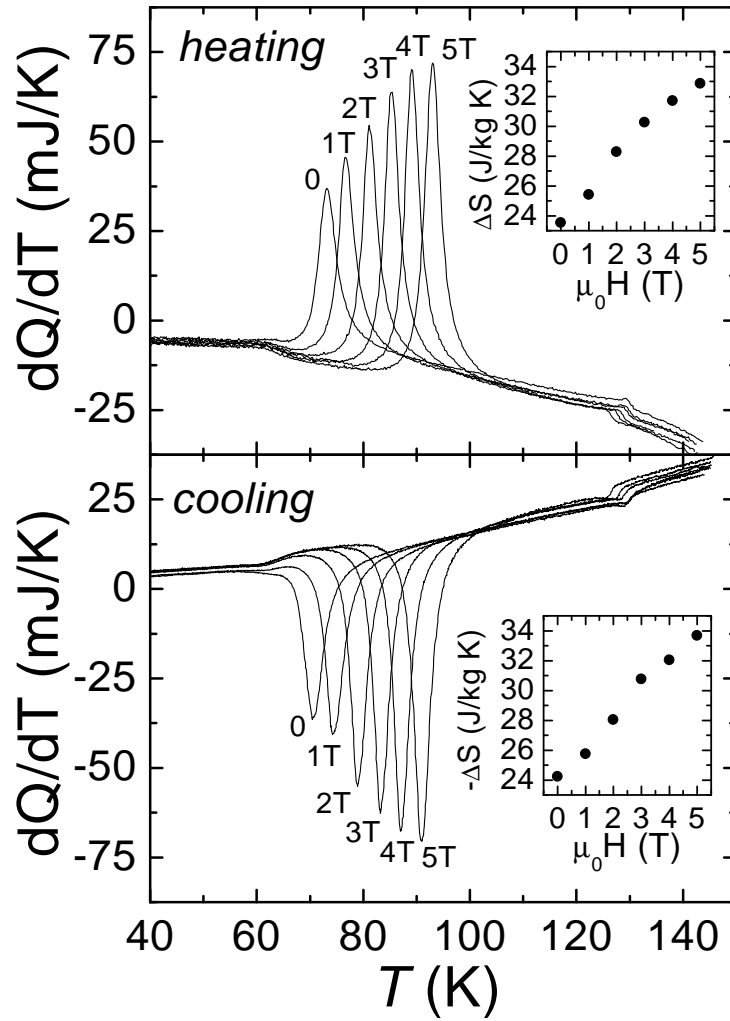


Figure 4.7: Calorimetric curves recorded sweeping T (on heating and cooling) in a $\text{Gd}_5(\text{Si}_{0.1}\text{Ge}_{0.9})_4$ sample (#1, as-cast) for different applied magnetic fields. Insets show the entropy change as a function of magnetic field.

and magnetic degrees of freedom. A thorough discussion of the measurements on the series of $\text{Gd}_5(\text{Si}_x\text{Ge}_{1-x})_4$ alloys will be given in the next chapters.

4.5 Results sweeping H

DSC are usually designed to continuously sweep the temperature while $\dot{Q}(t)$ and $T(t)$ are recorded. The T sweep induces thermally the first-order transition in the sample, which releases or absorbs heat. In the particular case of field-induced transitions, the temperature T_i of the peak of the transition in the calorimetric curve is tuned by the magnetic field, and consequently the field dependence of ΔS is obtained.

Besides, our new differential scanning calorimeter can also work sweeping the field. Fixing a temperature above T_i , a high enough magnetic field also induces the first-order transition. This fact gives rise to a *direct* measurement of the magnetocaloric effect, since the entropy change achieved by the application of a magnetic field can be measured. To our knowledge, this is the first time that ΔS can be measured *directly*. In this case, the heat flow $\dot{Q}(t)$ and the increasing/decreasing field $H(t)$ are recorded, leading to the magnetic field rate, dH/dt , and to the calorimetric curve $dQ/dH = \dot{Q} (dH/dt)^{-1}$. L and ΔS are thus given by:

$$L = \int_{H_L}^{H_H} \frac{dQ}{dH} dH ; \quad \Delta S = \frac{1}{T} \int_{H_L}^{H_H} \frac{dQ}{dH} dH = \frac{L}{T} , \quad (4.2)$$

where H_H and H_L are, respectively, fields above and below the starting and finishing transition fields. As the range of H is more restricted than that of T , therefore this kind of scannings are limited to a few temperatures above T_i . Figure 4.8 shows an example of the calorimetric curves recorded on increasing and decreasing H for a $\text{Gd}_5(\text{Si}_{0.05}\text{Ge}_{0.95})_4$ sample at different fixed temperatures above the zero-field transition temperature [$T_i(H=0) \cong 45$ K]. The main features of the transition are given in section 2.2. The transition field increases linearly with temperature, with a slope 5.0 ± 0.1 K/T, in excellent agreement with values obtained from both DSC sweeping T and magnetisation. In this sample, only curves at $T=50, 55$ and 60 K show the total completion of the transition and allow the transition peak to be integrated properly, in contrast with $T=65$ K, where it is clear that the maximum available field of 5 T is not high enough to complete the transition. The entropy change at the transition increases with T , as shown in the insets in Fig. 4.8, in agreement with the values obtained through DSC sweeping T . Curves at different field rates (0.1 and 1 T/min) for the same T yield the same values of L and ΔS within the experimental error, showing that measurements do not depend on the field rate. However, it is obvious that the actual dynamics of the transition is strongly affected by the field rate, and that avalanches are already discernible at

4.5. Results sweeping H

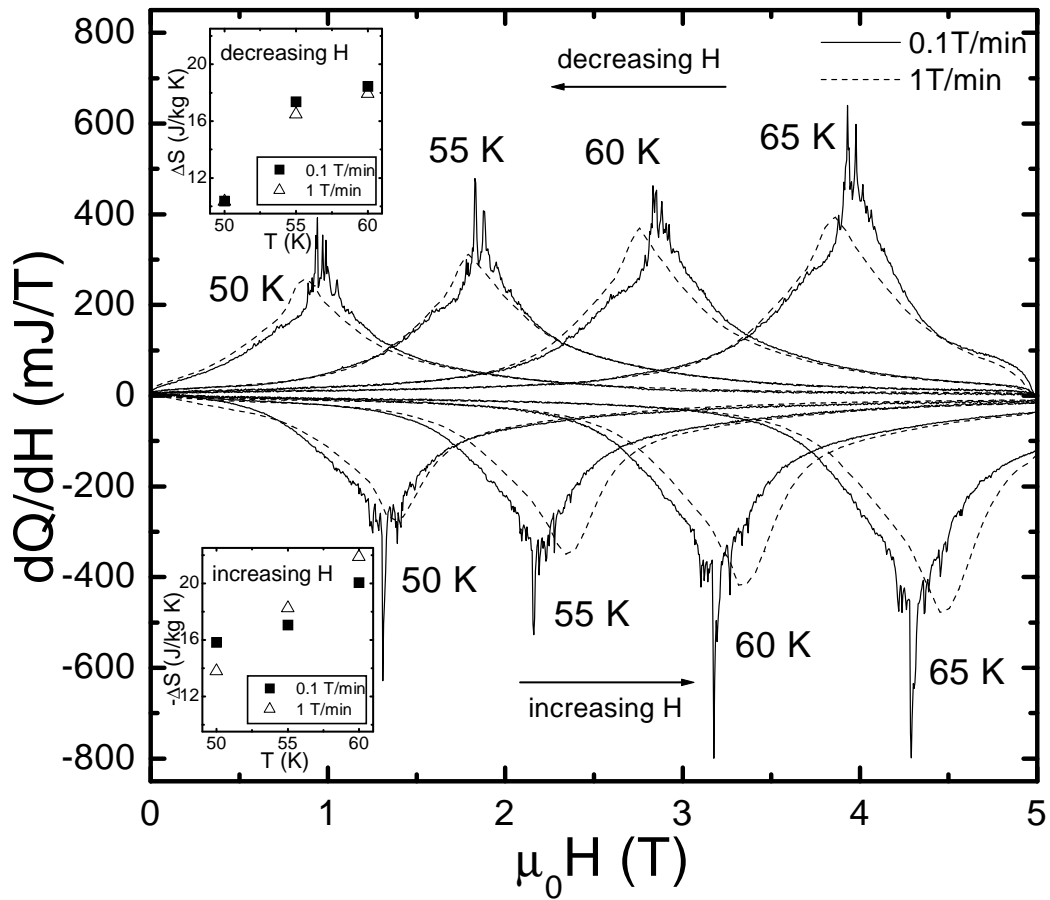


Figure 4.8: Calorimetric curves recorded sweeping H (increasing and decreasing H) in a $\text{Gd}_5(\text{Si}_{0.05}\text{Ge}_{0.95})_4$ sample (#1, T4+Q heat treatment) at some fixed temperatures and for two different field rates. Insets show the entropy change as a function of temperature for the different rates.

0.1 T/min (see Chapter 9). ΔS on increasing H is $\sim 2-4$ J/(kg K) larger than that on decreasing H . The detailed analysis of these data and those for the rest of the samples will be undertaken in the following chapters.

4.6 Conclusions

A new differential scanning calorimeter has been developed. The equipment features a high sensitivity down to 10 K and operates under applied magnetic fields of up to 5 T and within the temperature range 10-300 K. The device may be used to study first-order solid-solid phase transitions in the presence of magnetic fields. It has also been shown that this calorimeter enables an accurate determination of the entropy change in the magnetostructural phase transition of alloys exhibiting giant magnetocaloric effect, which can be induced sweeping either T or H . Therefore, it is expected that this kind of measurements will clarify the controversial issue of the actual value of the entropy change in the vicinity of a first-order transition.

Bibliography

- [1] For a recent review on calorimetry see Y. Kraftmakher, Phys. Rep. **356**, 1 (2002).
- [2] O.S. Gill, S.R Suerbrunn and M. Reading, J. Therm. Anal. **40**, 931 (1993).
- [3] I.K. Moon, D.H. Jung, K.-B. Lee and Y.H. Jeong, Appl. Phys. Lett **76**, 2451 (2000).
- [4] A.I. Kharkovski, Ch. Binek and W. Kleemann, Appl. Phys. Lett. **77**, 2409 (2000).
- [5] V.K. Pecharsky and K.A. Gschneidner, Jr., Phys. Rev. Lett. **78**, 4494 (1997).
- [6] A. Giguère, M. Földeàki, B. Ravi Gopal, R. Chahine, T.K. Bose, A. Frydman and J.A. Barclay, Phys. Rev. Lett. **83**, 2262 (1999).
- [7] K.A. Gschneider, Jr., V.K. Pecharsky, E. Brück, H.G.M. Duijn, and E. Levin, Phys. Rev. Lett. **85**, 4190 (2000).
- [8] J.R. Sun, F.X. Hu, and B.G. Shen, Phys. Rev. Lett. **85**, 4191 (2000).
- [9] M. Földeàki, R. Chahine, T.K. Bose, and J.A. Barclay, Phys. Rev. Lett. **85**, 4192 (2000).
- [10] V.K. Pecharsky, J.O. Moorman, and K.A. Gschneidner, Jr., Rev. Sci. Instr. **68**, 4196 (1997).
- [11] B.R. Gopal, R. Chahine, and T.K. Bose, Rev. Sci. Instr. **68**, 1818 (1997).
- [12] S. Yu. Dan'kov, A.M. Tishin, V.K. Pecharsky, and K.A. Gschneidner, Jr., Rev. Sci. Instr. **68**, 2432 (1997).
- [13] For a detailed explanation on the VTI, which controls the temperature of the sample by tuning high-purity helium pressure inside the sample calorimeter chamber, see B.J. Hattink, Ph. D. Thesis (chapter 2), Universitat de Barcelona, Catalonia, 2003.
- [14] S.M. Sarge, E. Gmelin, G.W.H. Höhne, H.K. Cammenga, W. Hemminger, and W. Eysel, Thermochim. Acta **247**, 129 (1994).
- [15] R. Romero and J.L. Pelegrina, Phys. Rev. B **50**, 9046 (1994).
- [16] A. Planes and Ll. Mañosa, Solid State Phys. **55**, 159 (2001).

CHAPTER 4. DESIGN OF A DSC WITH MAGNETIC FIELD

- [17] J. Ortín, *Thermochim. Acta* **121**, 397 (1987).
- [18] V.K. Pecharsky and K.A. Gschneidner, Jr., *Appl. Phys. Lett.* **70**, 3299 (1997).
- [19] L. Morellon, J. Blasco, P.A. Algarabel, and M. R. Ibarra, *Phys. Rev. B* **62**, 1022 (2000).